ISSN 1063-7826, Semiconductors, 2019, Vol. 53, No. 5, pp. 673–677. © Pleiades Publishing, Ltd., 2019.
Russian Text © The Author(s), 2019, published in Fizika i Tekhnika Poluprovodnikov, 2019, Vol. 53, No. 5, pp. 680–684.

XVI INTERNATIONAL CONFERENCE "THERMOELECTRICS AND THEIR APPLICATIONS–2018" (ISCTA 2018), ST. PETERSBURG, OCTOBER 8–12, 2018

Thermoelectric Properties of $Bi_{2-x}Lu_xTe_{2.7}Se_{0.3}$ Solid Solutions

A. E. Vasil'ev[a,*], M. N. Yapryntsev[a], O. N. Ivanov[a,b], and M. V. Zhezhu[a]

[a] *Belgorod National Research University, Belgorod, 308015 Russia*

[b] *Belgorod State Technological University named after V.G. Shukhov, Belgorod, 308012 Russia*

**e-mail: 748070@bsu.edu.ru*

Received December 20, 2018; revised December 24, 2018; accepted December 28, 2018

Abstract—The thermoelectric properties of compounds based on $Bi_{2-x}Lu_xTe_{2.7}Se_{0.3}$ solid solutions with $x = 0$, 0.05, 0.1, and 0.2 are studied. The samples for investigations are prepared by chemical-solution deposition (to synthesize the initial powders) and spark plasma sintering (to obtain bulk samples). The patterns of changes in the electrical resistivity, Seebeck coefficient, and total thermal conductivity of the samples are determined as a function of the lutetium content. It is established that the optimal combination of these thermoelectric characteristics is attained for the composition with $x = 0.05$, which demonstrates the highest thermoelectric figure of merit ($ZT \approx 0.9$ in the temperature range of 400–480 K) among all the studied compositions.

DOI: 10.1134/S1063782619050282

1. INTRODUCTION

The numerous advantages of thermoelectric generators, such as reliability, environmental friendliness, noiseless operation, and scaling capability are largely outweighed by their significant disadvantage, which is an extremely low efficiency usually not exceeding 10%. In turn, the efficiency of thermoelectric generators is determined by the thermoelectric figure of merit of the employed thermoelectric material, which can be expressed as $ZT = (S^2/\rho\kappa)T$, where S, ρ, and κ are the Seebeck coefficient, electrical resistivity, and total thermal conductivity of the material, respectively, and T is the absolute temperature. Evidently, an efficient thermoelectric material should possess both a high S value and low ρ and κ values. There is a narrow range of materials in which the combination of S, ρ, and κ proves to be acceptable for their practical application as thermoelectrics. At present, solid solutions with the composition $Bi_2Te_{2.7}Se_{0.3}$, exhibiting the electron conductivity type, are one such material for low-temperature thermoelectric applications. However, the thermoelectric figure of merit of these solid solutions is also not very high ($ZT \approx 1$), which considerably limits the potential of their wide application. Therefore, the search for scientific and technological ways to increase the thermoelectric figure of merit of $Bi_2Te_{2.7}Se_{0.3}$ compounds is a topical issue of both semiconductor physics and physical materials science.

Doping with different impurities often turns out to be a rather efficient way of optimizing the main thermoelectric characteristics (S, ρ, and κ), which promotes an increase in ZT of compounds based on bismuth telluride Bi_2Te_3 [1–3]. Recently, it was established that rare-earth elements are one of the most efficient dopants in the Bi_2Te_3 structure [4–12]. Unlike Bi_2Te_3, the effect of doping with various rare-earth elements on the thermoelectric properties of $Bi_2Te_{2.7}Se_{0.3}$ solid solutions is studied far less [13, 14], which became the impetus for investigations, the results of which are presented here.

2. EXPERIMENTAL

The initial powder compounds based on $Bi_{2-x}Lu_xTe_{2.7}Se_{0.3}$ with $x = 0$, 0.05, 0.1, and 0.2 were synthesized by the technique of chemical deposition from a solution. This procedure for synthesis allows one, firstly, to obtain powder particles with various sizes in a controlled way by varying the solvent composition and, secondly, allows a considerable decrease in the temperature of synthesis compared to the classical technique of alloying in a quartz cell.

For synthesis, high-purity reagents were used: bismuth oxide (Bi_2O_3 99.9%), tellurium oxide (TeO_2 99.9%), selenium oxide (SeO_2 99.9%), lutetium acetate ($Lu(CH_3COO)_3$ 99.9%), potassium hydroxide (KOH 99.9%), and ethylene glycol (1,2-ethylene glycol 99.8%). The precursors for synthesis taken in stoichiometric proportion in accordance with x were placed in a conical flask equipped with a reflux condenser. The reaction was carried out at the boiling temperature of the reaction mixture (~195°C) with

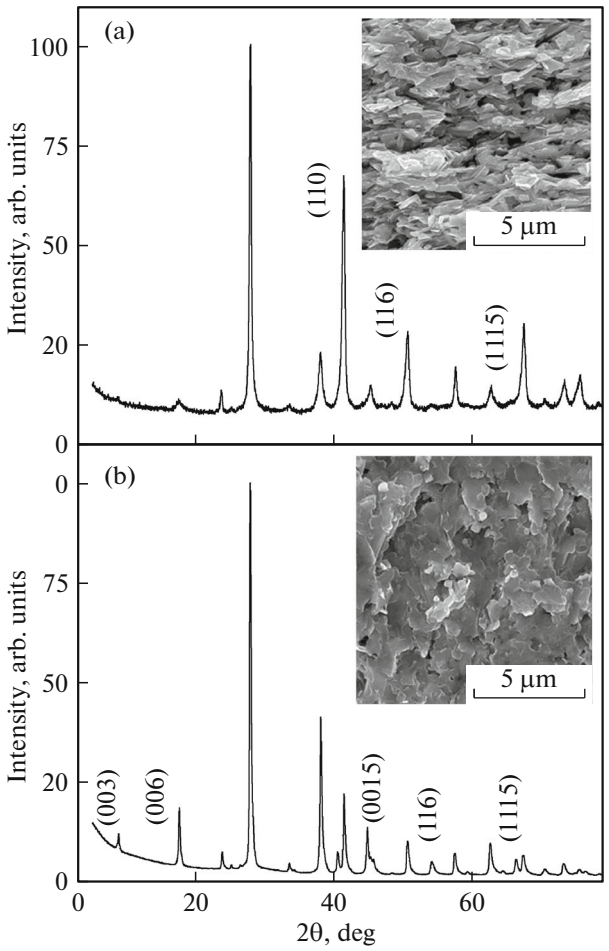

Fig. 1. Diffraction patterns recorded from surfaces of the sample with $x = 0.05$ oriented (a) perpendicular or (b) parallel to the pressing direction in the process of spark plasma sintering. In the insets, SEM images of the surfaces are shown.

constant stirring for 24 h. After termination of the reaction, the obtained powders were filtered, washed with water and isopropyl alcohol to remove organic and inorganic admixtures, and, finally, dried in a vacuum cabinet for 12 h.

Compaction of the bulk samples was carried out by means of spark plasma sintering of the initial powders (SPS-25/10 system) at a pressure of 40 MPa and temperature of 780 K for 5 min.

The phase composition of both initial powders and bulk samples was investigated by X-ray phase analysis (Ultima IV Rigaku diffractometer; the parameters of the investigations: the range of angles $2\theta = 10°–80°$, a step of 0.02, and a rate of 1 deg min^{-1}).

To study the morphology of the initial powders and determine the average powder particle size, transmission electron microscopy was employed (a Jeol 2100 microscope).

The features of the microstructure of the bulk samples were investigated by scanning electron microscopy (SEM) on a Quanta 600 microscope. The elemental composition of the samples was determined with the help of energy-dispersive analysis (EDAX detector).

The electrical conductivity and Seebeck coefficient of the bulk samples were measured in the temperature range from 300 to 600 K in a helium atmosphere (a ZEM-3 unit).

In the same temperature range, the thermal conductivity of the bulk samples was determined using the laser flash method (TC-1200 system).

3. EXPERIMENTAL RESULTS

According to the data of transmission electron microscopy, the synthesized powders of compounds $Bi_{2-x}Lu_xTe_{2.7}Se_{0.3}$ with $x = 0$, 0.05, 0.1, and 0.2 consisted of particles in the form of hexagonal wafers with an average size of ~200 nm. The synthesized powders of all compositions were single phase and possessed a rhombohedral crystal structure (space group $R\bar{3}m$).

To prepare the bulk materials, the synthesized powders were compacted by spark plasma sintering. According to the data of X-ray phase analysis, the bulk samples with all compositions were single phase and possessed a rhombohedral crystal structure as well. The unit-cell parameters for all samples were almost independent of x and were determined as $c = 30.35$ Å and $a = b = 4.35$ Å. The composition independence of these parameters is due to a small difference in the covalent radii of Lu (1.75 Å) and Bi (1.60 Å) [15].

According to the data of energy-dispersive analysis, the actual elemental compositions for all bulk samples $Bi_{2-x}Lu_xTe_{2.7}Se_{0.3}$ corresponded to nominal compositions with $x = 0$, 0.05, 0.1, and 0.2.

It was established that bulk samples with all compositions have a pronounced texture featuring the preferential orientation of grains in the samples after spark plasma sintering. The presence of texture is seen from considerable differences in the diffraction patterns recorded from the surfaces of the samples oriented either perpendicularly or parallel to the pressing direction in the process of sintering. By way of example, such diffraction patterns for the composition with $x = 0.05$ are shown in Figs. 1a and 1b, respectively. In the diffraction pattern of Fig. 1a, one can observe an increased height of the peaks corresponding to reflection from planes (00l), whereas, in the diffraction pattern of Fig. 1b, an increased intensity is typical of the peaks corresponding to reflection from planes (11l). The redistribution of the intensity of the peaks is due to such an orientation of the grains in the bulk materials that the crystallographic axis c of the grains is oriented predominantly parallel to the pressing direction upon spark plasma sintering, and the plane a–b is oriented perpendicular to this direction.

The degree of the preferential orientation of grains can be estimated with the help of the orientation factor [16]

$$f = \frac{p - p_0}{1 - p_0}, \quad (1)$$

where p and p_0 are determined as

$$p = \frac{I(00l)}{\Sigma I(hkl)}, \quad p = \frac{I_0(00l)}{\Sigma I_0(hkl)}. \quad (2)$$

Here, I and I_0 are the intensities of the peaks for the oriented (textured) and unoriented (nontextured) samples, respectively. In the ideal case, $f = 1$ for a completely oriented sample (single crystal) and $f = 0$ for a completely unoriented sample (powder or polycrystalline material with absolutely random grain orientation). For all the studied bulk samples $Bi_{2-x}Lu_xTe_{2.7}Se_{0.3}$ with $x = 0$, 0.05, 0.1, and 0.2, the orientation factor was ~0.5.

The presence of texture in these samples is also corroborated by the data of scanning electron microscopy. It was established that the grains have a platelet shape, with these platelets laying primarily in the plane perpendicular to the pressing direction upon spark plasma sintering. For all sample compositions, the length of the platelets (grains) was ~400 nm and their width was ~50 nm. For illustration, SEM images of the grain structure of the sample with $x = 0.05$ obtained from the surface parallel or perpendicular to the pressing direction are shown in the insets to Figs. 1a and 1b, respectively.

It is noteworthy that both bismuth telluride and solid solutions based on it feature strong anisotropy of the transport properties, such as electrical conductivity and thermal conductivity [17]; i.e., these characteristics measured along the rhombohedral c axis differ greatly from the properties measure in the a–b plane oriented perpendicular to the c axis. In polycrystalline materials with a random grain orientation, anisotropy of the properties is suppressed. In textured samples, anisotropy of the thermoelectric properties, typical of single crystals, is "reduced" in part; i.e., the thermoelectric figure of merit measured parallel or perpendicular to the texture axis can differ noticeably [18]. Since the task of investigating the anisotropy of the thermoelectric properties of textured samples of $Bi_{2-x}Lu_xTe_{2.7}Se_{0.3}$ solid solutions with various x was beyond the scope of this work, the thermoelectric characteristics of these samples were further measured in only one direction, viz., the direction perpendicular to the pressing direction upon spark plasma sintering (in the a–b plane). Of note, the thermoelectric figure of merit of textured samples of bismuth telluride and solid solutions based on it are considerably higher for this direction than that determined for the direction coinciding with the pressing direction (along the c axis) [18].

The temperature dependences of ρ, S, κ, and ZT of the $Bi_{2-x}Lu_xTe_{2.7}Se_{0.3}$ samples with $x = 0$, 0.05, 0.1, and 0.2 are shown in Fig. 2. In the studied temperature range, the electrical resistivity of the samples with all compositions increases with increasing temperature (Fig. 2a). Such behavior is typical of degenerate semiconductors (among which are the investigated solid solutions) and metals. In this case, the temperature dependence of ρ is determined by the temperature dependence of the electron mobility (the concentration of electrons is almost independent of temperature). At temperatures higher than room temperature, the main temperature-dependent mechanism of the scattering of electrons, determining their mobility, is scattering at acoustic and optical phonons. More importantly, the electrical resistivity of the samples increases successively with an increase in x. This means that Lu atoms substituting Bi atoms in the $Bi_2Te_{2.7}Se_{0.3}$ structure are efficient scattering centers for electrons.

The effect of lutetium doping on the Seebeck coefficient of the studied samples is much less pronounced compared to this effect on the electrical resistivity (Fig. 2b). It should be noted right away that, for all the samples, the Seebeck coefficient has a negative sign, which is typical of solids with the electron conductivity type. As is seen from Fig. 2b, with an increase in the lutetium content, S decreases slightly. The Seebeck coefficient for degenerate semiconductors is determined in accordance with the expression

$$S = \frac{2k_B T m^*}{3e\hbar^2}\left(\frac{\pi}{3n}\right)^{2/3}\left(\frac{3}{2} + \gamma\right), \quad (3)$$

where k_B is the Boltzmann constant, $\hbar$ is Planck's constant, n is the concentration of electrons, e is the elementary charge, m^* is the effective mass of the density of states for electrons, and γ is the scattering factor.

According to Eq. (3), a change in the S value of the $Bi_{2-x}Lu_xTe_{2.7}Se_{0.3}$ samples with various x can be caused by a change in the concentration of electrons, the scattering factor, and effective mass of the density of states for electrons (e.g., in the case of the formation of an impurity band associated with Lu with a drastic change in the density of states in the vicinity of the Fermi level). The broad maxima observed in the $S(T)$ curves at a temperature of ~480 K are due to the onset of intrinsic conductivity in the investigated samples at this temperature [18]. In this case, the thermal generation of electron–hole pairs takes place, with the Seebeck coefficient being positive for hole-type conductivity.

Lutetium doping had a considerable effect on the total thermal conductivity of the $Bi_{2-x}Lu_xTe_{2.7}Se_{0.3}$ samples (Fig. 2c). In the whole studied temperature range, the thermal conductivity falls with a gradual increase in x. Such a behavior can be associated with a decrease in both the electron contribution (since the electrical resistivity of the samples rises with an

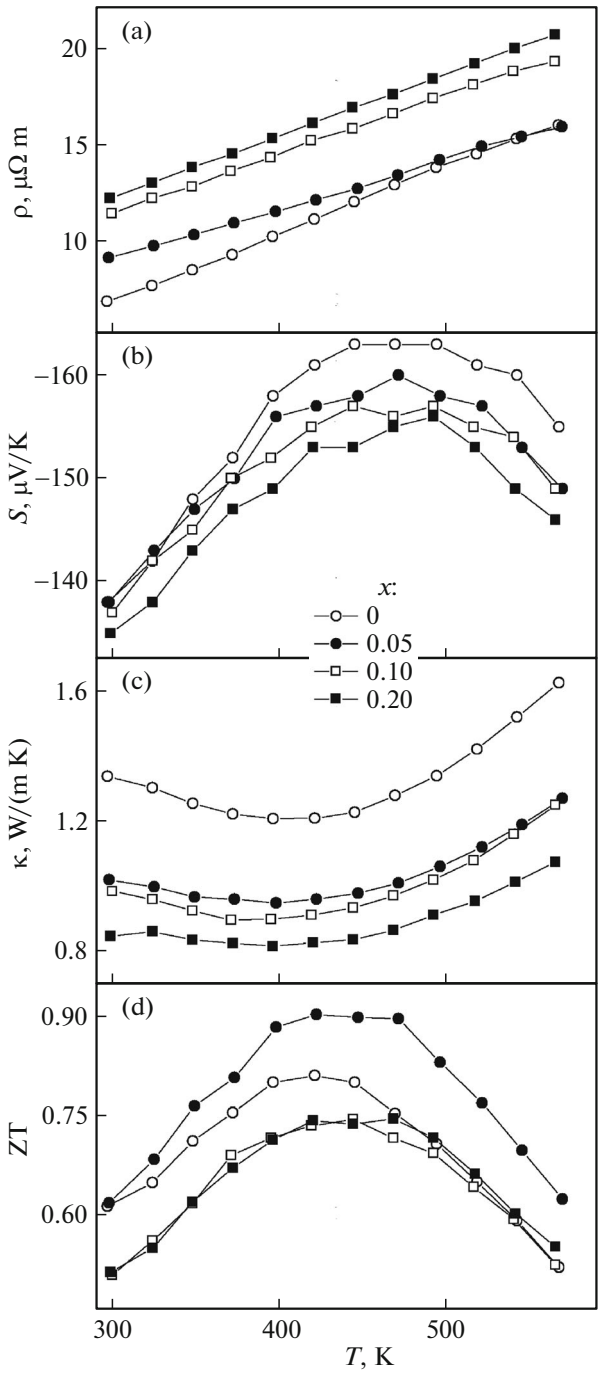

Fig. 2. Temperature dependences (a) of the electrical resistivity, (b) Seebeck coefficient, (c) total thermal conductivity, and (d) thermoelectric figure of merit of the samples with different compositions.

increase in x) and the phonon contribution to the total thermal conductivity, since Lu atoms in the $Bi_2Te_{2.7}Se_{0.3}$ structure can be efficient centers of scattering for short-wavelength phonons. In the process of carrying out this work, the electron and phonon contributions to the total thermal conductivity were not separated.

In addition, the emergence of a minimum in the $\kappa(T)$ curves at a temperature of ~400 K should be noted. The appearance of this minimum is due to a change in the mechanism of thermal conductivity. For the studied temperature range, a decrease in κ with an increase in the temperature below the temperature minimum is due to a decrease in the phonon mean free path, and an increase in κ above the minimum temperature is due to the appearance of a bipolar component of the thermal conductivity. For bipolar thermal conductivity, at the hot end of the sample, electron–hole pairs are generated, which diffuse toward the cold end, where they recombine; in the process of the recombination of one electron–hole pair, energy is released, which is nearly equal to the band-gap energy [19].

The temperature dependences of the thermoelectric figure of merit of $Bi_{2-x}Lu_xTe_{2.7}Se_{0.3}$ obtained using the $\rho(T)$, $S(T)$, and $\kappa(T)$ dependences are shown in Fig. 2d. The composition with $x = 0.05$ has a thermoelectric figure of merit of $ZT \approx 0.9$ in the temperature range of 400–480 K, which is higher than the thermoelectric figure of merit of undoped bismuth telluride ($ZT \approx 0.77$ for the same temperature range). The maximum thermoelectric figure of merit of the compositions with $x = 0.1$ and 0.2 does not exceed 0.74. Comparing the effect of lutetium doping on the thermoelectric properties of $Bi_2Te_{2.7}Se_{0.3}$, it is necessary to mention that, although, for the composition with $x = 0.05$, the electrical resistivity increases and the Seebeck coefficient decreases relative to the corresponding values for undoped bismuth telluride (which leads to a decrease in ZT), the decrease in the total thermal conductivity (encouraging an increase in ZT) proves to be so significant that the final thermoelectric figure of merit turns out to be higher than ZT of undoped $Bi_2Te_{2.7}Se_{0.3}$. For compositions with $x = 0.05$ and 0.2, an increase in ρ and a decrease in S affect ZT to a much greater degree than a decrease in κ does; therefore, the final ZT values are lower than the thermoelectric figure of merit of undoped $Bi_2Te_{2.7}Se_{0.3}$.

4. CONCLUSIONS

The patterns of changes in the electrical resistivity, Seebeck coefficient, and total thermal conductivity of compounds based on $Bi_{2-x}Lu_xTe_{2.7}Se_{0.3}$ solid solution with $x = 0$, 0.05, 0.1, and 0.2 were established. It was shown that, for the composition with $x = 0.1$, the thermoelectric figure of merit is higher and, for the compositions with $x = 0.1$ and 0.2, it is smaller relative to the thermoelectric figure of merit of undoped bismuth telluride.

Investigation of the anisotropy of the thermoelectric properties of the samples and determination of the mechanisms of the effect that lutetium doping has on these properties will be the subjects of further research.

FUNDING

The work was carried out under financial support of the Ministry of Education and Science of the Russian Federation, project no. 3.6586.2017/6.7. In the research, equipment of the shared facilities "Technologies and Materials" of Belgorod National Research University was used.

REFERENCES

1. Y. Pan, T. R. Wei, C. F. Wu, and J. F. Li, J. Mater. Chem. C **3**, 10583 (2015).
2. L. Hu, T. Zhu, X. Liu, and X. Zhao, Adv. Funct. Mater. **24**, 5211 (2014).
3. J. Suh, K. M. Yu, D. Fu, X. Liu, F. Yang, J. Fan, D. J. Smith, Y. H. Zhang, J. K. Furdyna, C. Dames, W. Walukiewicz, and J. Wu, Adv. Mater. **27**, 3681 (2015).
4. J. Yang, F. Wu, Z. Zhu, L. Yao, H. Song, and X. Hu, J. Alloys Compd. **619**, 401 (2015).
5. X. H. Ji, X. B. Zhao, Y. H. Zhang, B. H. Lu, and H. L. Ni, J. Alloys Compd. **387**, 282 (2005).
6. F. Wu, H. Song, J. Jia, and X. Hu, Prog. Nat. Sci. Mater. Int. **23**, 408 (2013).
7. F. Wu, W. Shi, and X. Hu, Electron. Mater. Lett. **11**, 127 (2015).
8. X. H. Ji, X. B. Zhao, Y. H. Zhang, B. H. Lu, and H. L. Ni, Mater. Lett. **59**, 682 (2005).
9. F. Wu, H. Z. Song, J. F. Jia, F. Gao, Y. J. Zhang, and X. Hu, Phys. Status Solidi A **210**, 1183 (2013).
10. W. Y. Shi, F. Wu, K. L. Wang, J. J. Yang, H. Z. Song, and X. J. Hu, J. Electron. Mater. **43**, 3162 (2014).
11. X. B. Zhao, Y. H. Zhang, and X. H. Ji, Inorg. Chem. Commun. **7**, 386 (2004).
12. O. Ivanov, M. Yaprintsev, R. Lyubushkin, and O. Soklakova, Scr. Mater. **146**, 91 (2018).
13. J. Yang, F. Wu, Z. Zhu, L. Yao, H. Song, and X. Hu, J. Alloys Compd. **619**, 401 (2015).
14. R. Cao, H. Song, W. Gao, E. Li, X. Li, and X. Hu, J. Alloys Compd. **23**, 408 (2013).
15. Y. Q. Jia, J. Solid State Chem. **95**, 184 (1991).
16. X. A. Fan, J. Y. Yang, R. G. Chen, H. S. Yun, W. Zhu, S. Q. Bao, and X. K. Duan, J. Phys. D: Appl. Phys. **39**, 740 (2006).
17. T. Caillat, M. Carle, P. Pierrat, H. Scherrer, and S. Scherrer, J. Phys. Chem. Solids **53**, 1121 (1992).
18. A. Vasil'ev, M. Yaprintsev, O. Ivanov, and E. Danshina, Solid State Sci. **84**, 28 (2018).
19. S. Wang, J. Yang, T. Toll, J. Yang, W. Zhang, and X. Tang, Sci. Rep. **5**, 10136 (2015).

Translated by Z. Smirnova